materials

MDPI

Article

The Effect of Different Morphologies of WO_3/GO Nanocomposite on Photocatalytic Performance

Banu Esencan Türkaslan [1,*], Aziz Kerim Çelik [1], Ayça Dalbeyler [1] and Nicholas Fantuzzi [2]

[1] Department of Chemical Engineering, Faculty of Engineering, University of Süleyman Demirel, Isparta 32260, Turkey
[2] Department of Civil, Chemical, Environmental, and Materials Engineering, University of Bologna, 40126 Bologna, Italy
* Correspondence: banuturkaslan@sdu.edu.tr

Abstract: Tungsten trioxide/graphene oxide (WO_3/GO) nanocomposites have been successfully synthesized using in situ and ex situ chemical approaches. Graphite and tungsten carbide (WC) were employed to perform in situ synthesis, and WO_3 and GO were employed to perform the ex situ synthesis of WO_3/GO nanocomposites. GO, which was required for ex situ synthesis, is synthesized via the modified and improved Hummers method. XRD, SEM/EDS, and FTIR are used for the characterization of the nanocomposite. From the XRD of the WO_3/GO nanocomposites, it was observed that WO_3 distributed uniformly on graphene oxide sheets or was incorporated between the sheets. The photocatalytic activities of WO_3/GO nanocomposites were evaluated by methylene blue (MB) adsorption and visible light photocatalytic degradation activities by UV-vis spectroscopy. The results showed that the efficiency of the photocatalytic activity of the nanocomposite depends on different synthesis methods and the morphology resulting from the changed method. WO_3/GO nanocomposites synthesized by both methods exhibited much higher photocatalytic efficiencies than pure WO_3, and the best degradation efficiencies for MB was 96.30% for the WO_3/GO in situ synthesis nanocomposite.

Keywords: tungsten trioxide; graphene oxide; photocatalysis; nanocomposite

Citation: Esencan Türkaslan, B.; Çelik, A.K.; Dalbeyler, A.; Fantuzzi, N. The Effect of Different Morphologies of WO_3/GO Nanocomposite on Photocatalytic Performance. *Materials* **2022**, *15*, 8019. https://doi.org/10.3390/ma15228019

Academic Editor: Michela Alfè

Received: 7 October 2022
Accepted: 9 November 2022
Published: 14 November 2022

1. Introduction

In recent years, due to a notable increase in industrial activities that produce wastewater, the development of easily accessible adsorbent materials for cleaning water resources gained great momentum. Organic dyes have a dangerous and toxic effect on humans, which are found in the wastewater of various industries [1].

Among the different methods, degradation by photocatalysis has become a promising technique as it is simple and sustainable, and it enables the conversion of dyes to non-hazardous waste.

Nanocomposite materials, including metal oxide nanoparticles, with their advanced physicochemical properties, are common photoactive semiconductor materials that make them suitable for use in photocatalysis [2,3].

Tungsten oxide (WO_3), a nanostructured metal oxide, is widely used in the fields of gas detection [4,5], lithium-ion batteries [6,7], smart windows [8], and photocatalysis [9,10] practices. However, minimal photonic efficiency, the fast recombination rate of the charge carriers (photogenerated hole–electron), and low absorption ranges restrict the performance of WO_3 as an efficient photocatalyst [11–14]. The most important features that distinguish an ideal adsorbent from others are high adsorption capacity, rapid adsorption rate, and high selectivity. In this sense, doping WO_3 with other elements or compounds to improve its photocatalytic activity is deemed as an effective approach [15–17]. This may help improve the morphology of WO_3 material as well as the affected band levels and characteristics of the charge carriers [18].

In particular, graphene and its derivatives are frequently preferred in improving the performance of metal oxide nanostructures due to their extraordinary properties [19–21].

Contrary to graphene, the use of hydrophilic GO, which contains various proportions of carbon, oxygen, and hydrogen in its structure, is expanding day by day due to its easy dispersion in solutions, its dielectric properties, transparency and adjustable electronic properties [22,23]. However, it is difficult to separate GO from water after adsorption. To overcome this drawback, the hybridization of GO with other inorganic or organic materials is an alternative [24].

Hummers and Offeman synthesized GO via the method of oxidizing graphite in H_2SO_4, $NaNO_3$, and $KMnO_4$ atmospheres in 1958 [25]. Hummers' methodology was widely accepted, yet many disadvantages of this method have been reported, such as the production of toxic gas (NO_2 and N_2O_4), the residual nitrate, and low efficiency levels. In the last 20 years, alternative methods have been attempted relative to Hummer's method, including the addition of a peroxidation phase before $KMnO_4$ oxidation (without $NaNO_3$), increasing the amount of $KMnO_4$ rather than $NaNO_3$, and replacing $KMnO_4$ with K_2FeO_4 when $NaNO_3$ is extracted [26,27].

Studies conducted on WO_3/GO show that while the photocatalytic degradation activities of composites formed by combining WO_3 and GO structures that are synthesized separately via the ex situ method [28–32], there are no studies conducted regarding the photocatalytic degradation activities of nanocomposite structures, which are synthesized via in situ methods. It is thought that the composite structures synthesized using different methods are in the form of nanoparticles and nanowires [33–36], and this will affect the photocatalytic efficiency level.

In this study, highly efficient photocatalysts were developed, which is a method of producing renewable energy. To this end, both ex situ and in situ syntheses of WO_3/GO composites were performed, and the photocatalytic activity of the formed structure was examined. GO was synthesized via the modified and improved Hummers method without using $NaNO_3$. Given that there is no other WO_3/GO study conducted to examine the photocatalytic degradation activity of nanocomposite structures synthesized via in situ methods, our study bears the characteristics of the first study conducted in this field, and it is also the first study that compares photocatalytic activities of ex-situ and in-situ synthesized WO_3/GO composite structures.

2. Materials and Methods

Graphite flake (≥75% min), sulfuric acid (H_2SO_4, 98%), potassium permanganate ($KMnO_4$, 99%), hydrogen peroxide (H_2O_2, 30%), hydrochloric acid (HCI, 37%), and tungsten (VI) oxide (WO_3, <100 nm) were obtained from Sigma-Aldrich, and tungsten carbide (WC 45 nm, 99%) was obtained for the synthesis process from Nanokar company (İstanbul, Turkey).

2.1. Graphene Oxide (GO) Synthesis

GO was synthesized from layered graphite via the modified and improved Hummers method. Firstly, graphite (2 g) and then $KMnO_4$ (6 g) were gradually added into H_2SO_4 within the ice bath and mixed. Later, 300 mL of deionized water was added to the mixture. In order to stop the oxidation process and remove the impurities in the structure, the mixture was filtered by adding H_2O_2 and HCl, respectively. Synthesized graphite oxide measuring 1 g was taken into 350 mL of pure water and dispersed for 3 h. After two hours of sonication in order to facilitate the exfoliation of clumped graphite oxide layers on GO layers, the mixture was centrifuged, and GO was produced.

2.2. In Situ and Ex Situ Synthesis of WO_3/GO Composites

A total of 10 mg WO_3 and 30 mg GO were separately mixed for 2 h in 10 mL and 30 mL water, respectively, for the ex situ synthesis of WO_3/GO nanocomposites. Later, the

two solutions were combined and mixed for another 2 h in a magnetic stirrer. The achieved solution was centrifuged and finally dried at 60 °C for 24 h to obtain the WO_3/GO composite.

WC powder measuring 1 g and 10 mL H_2SO_4 were mixed in ice bath for the in situ synthesis of WO_3/GO nanocomposite. $KMnO_4$ measuring 3 g was gradually added into this mixture by continuously stirring. After adding $KMnO_4$, the mixture was stirred for an additional 2 h; then, 15 mL H_2O_2 (%30 *w*/*w*) was added, and it was observed that the color of the mixture turned bright yellow. The achieved solution was centrifuged and finally dried at 60 °C for 24 h.

2.3. Photocatalytic Activities of WO_3/GO Composites

Methylene blue (MB) was used as typical pollutants to study the photocatalytic activity of the synthesized WO_3/GO composites, which are synthesized with in situ and ex situ methods. In order to simulate the coloring agent, 75 mL of 20 ppm MB solutions was prepared. WO_3 was added to one of the solutions, and 15 mg of in situ WO_3/GO and 15 mg of ex situ WO_3/GO were added to other solutions as catalysts. Then, the solution was deposited into tubes in equal amounts in order to be able to make measurements at different time intervals.

After mixing for 30 min in the dark to ensure an adsorption–desorption balance, the solution tubes that were placed in the UV cabinet were exposed to a total of 2 xenon lamps, each of which was 150 Watt (Figure 1).

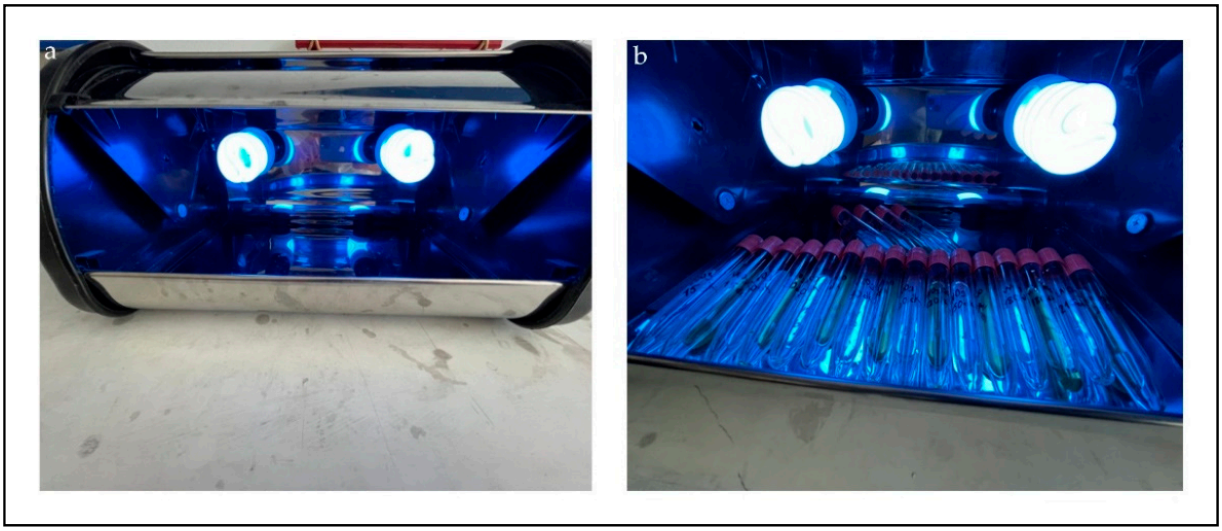

Figure 1. Designed UV cabinet (**a**) and tubes prepared for measurements to be made with different time intervals (**b**).

The distance between the lamp and the center of the tubes was measured as 8 cm. Samples were then taken at regular intervals to observe the degradation of methylene blue at 660 nm. The first measurement was made in the 15th minute; the next measurements were set to be made every 30 min, and regular measurements were made.

3. Results

The GO characterization was performed with X-ray diffraction (XRD) and the scanning electron microscopy (SEM/EDS) technique. WO_3/GO composites were also evaluated by using a scanning electron microscope (SEM, Quanta Feg 250; FEI, Eindhoven, the Netherlands). WO_3/GO composites were examined with a low-vacuum at 20.00 kV and 12.7–13.2 mm working distance at 5000× and 10000× magnifications, respectively. The elemental analysis of nanocomposites was carried out using an SEM microscope equipped with an energy-dispersive X-ray spectroscopy (EDX, Quanta Feg 250; FEI, Eindhoven, The Netherlands). The distribution and atomic composition of WO_3/GO was examined

using elemental mappings at an accelerating voltage of 20 kV. The crystalline phase of WO_3/GO were examined by X-ray diffraction (XRD, Bruker D8 Advance Twin-Twin; Bruker, Karlsruhe, Germany) at 40 kV, 40 mA, and 1600 watts. In order to determine the photocatalytic capacity of WO_3/GO nanocomposites, a UV-Vis spectrophotometer (UV-Vis Carry 60) device was used.

3.1. Characterization of GO

When the XRD spectrum of the GO structure was examined, it was observed that the peak formed at 2θ = 11.52° for GO, which is consistent with the results in the literature and it shows that the GO structure is obtained properly (Figure 2) [37].

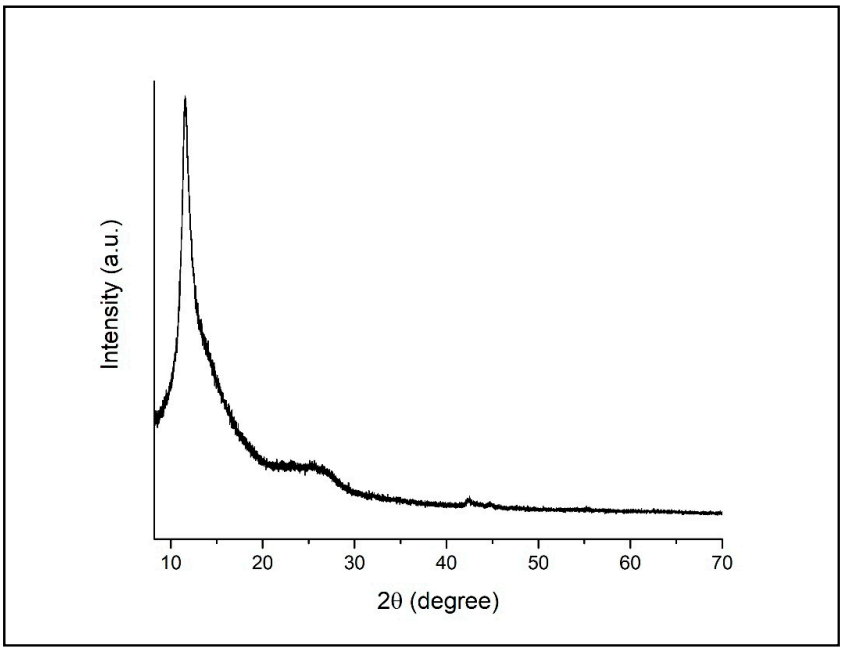

Figure 2. XRD patterns of GO.

SEM analysis results showed that the GO structure was formed by layered wavy structures piled on top of each other (Figure 3).

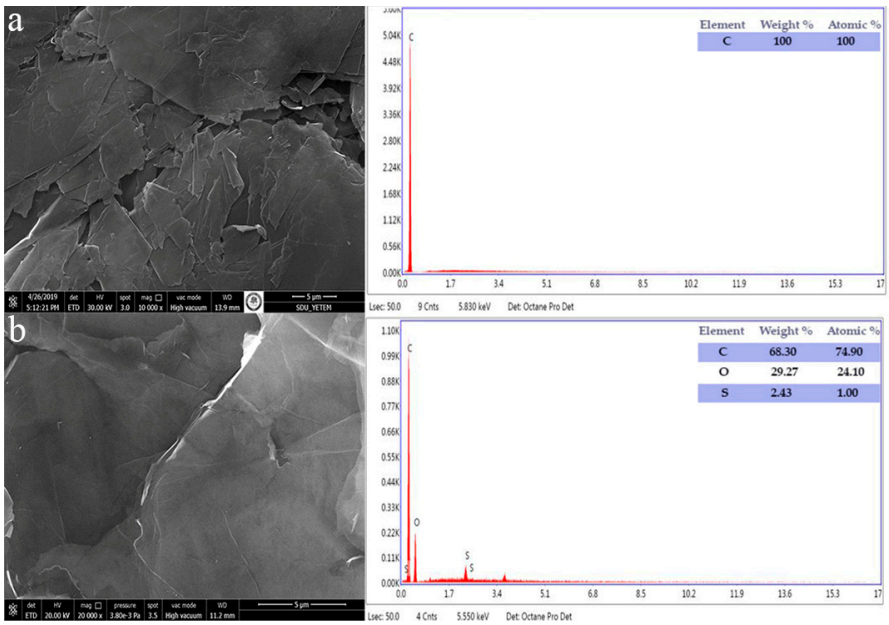

Figure 3. SEM/EDS image of (**a**) graphite and (**b**) GO.

3.2. Characterization of WO_3/GO Composites

Figure 4 provides the comparative FTIR spectra of GO and WO_3/GO composites. The peaks of <1000 cm^{-1} within the composite structures show the existence of pure WO_3 [28].

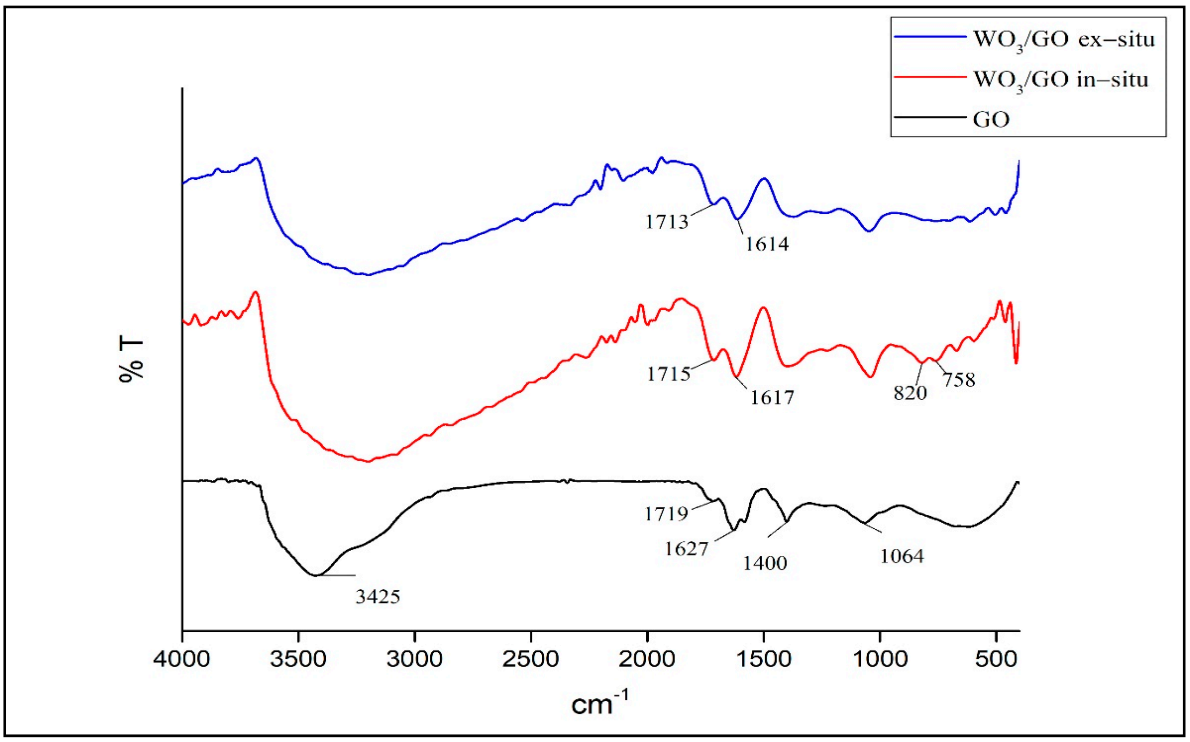

Figure 4. FTIR Spectra of GO and WO_3/GO Composites.

The FTIR spectrum of GO shows that the hydroxyl bond (-OH) is at 3425 cm^{-1}, the carbonyl bond (C=O) is at 1719 cm^{-1}, the aromatic bond (C=C) is at 1627cm^{-1}, the epoxy bond is at 1627 cm^{-1}, (C-O) is at 1400 cm^{-1}, and the alkoxy bond (C-O) is at 1064 cm^{-1}. The bands at 1715 cm^{-1} and 1617 cm^{-1} in the in situ synthesized composite structure and the bands at 1713 cm^{-1} and 1614 cm^{-1} in the ex situ synthesized composite structure belong to C=O and C=O vibrations, indicating the presence of GO in the composite's structure.

Peaks under <1000 cm^{-1} observed in composites that are not observed in GO structure are caused by O-W-O stretch vibrations and show that nanoparticles bind to GO nanolayers strongly [38]. O-W-O vibrations observed approximately at 820 and 758 cm^{-1} in the in situ synthesized composite structure were observed less in ex situ structures.

SEM micrographs were used to identify the morphology of the synthesized composites and the location of the metal oxide in the carbon matrix. It was observed that while the pure WO_3 structure comprised spongy structures of various sizes placed in such a way as to form spaces between them, WC consisted of randomly distributed and irregularly shaped coarse grains (Figure 5).

It is observed that the wavy interlayer spaces in GO structures are randomly dispersed by some spherical WO_3 particles to form smoother surfaces in the WO_3/GO ex situ synthesized nanocomposite (Figure 5e,f) structures. In WO_3/GO insitu synthesis morphologies, however, it is seen that a single-phase homogeneous composite morphology formed with good interfacial interaction between GO and WC (Figure 5g,h). The homogeneous coating of the GO surface with WO_3 as a result of good interfacial interaction in the in situ synthesis structure shows parallelisms with the O-W-O vibration bands observed in the FTIR results, while the lesser observation of these bands in the ex situ synthesis also supports the WO_3 particle structure observed between the GO layers.

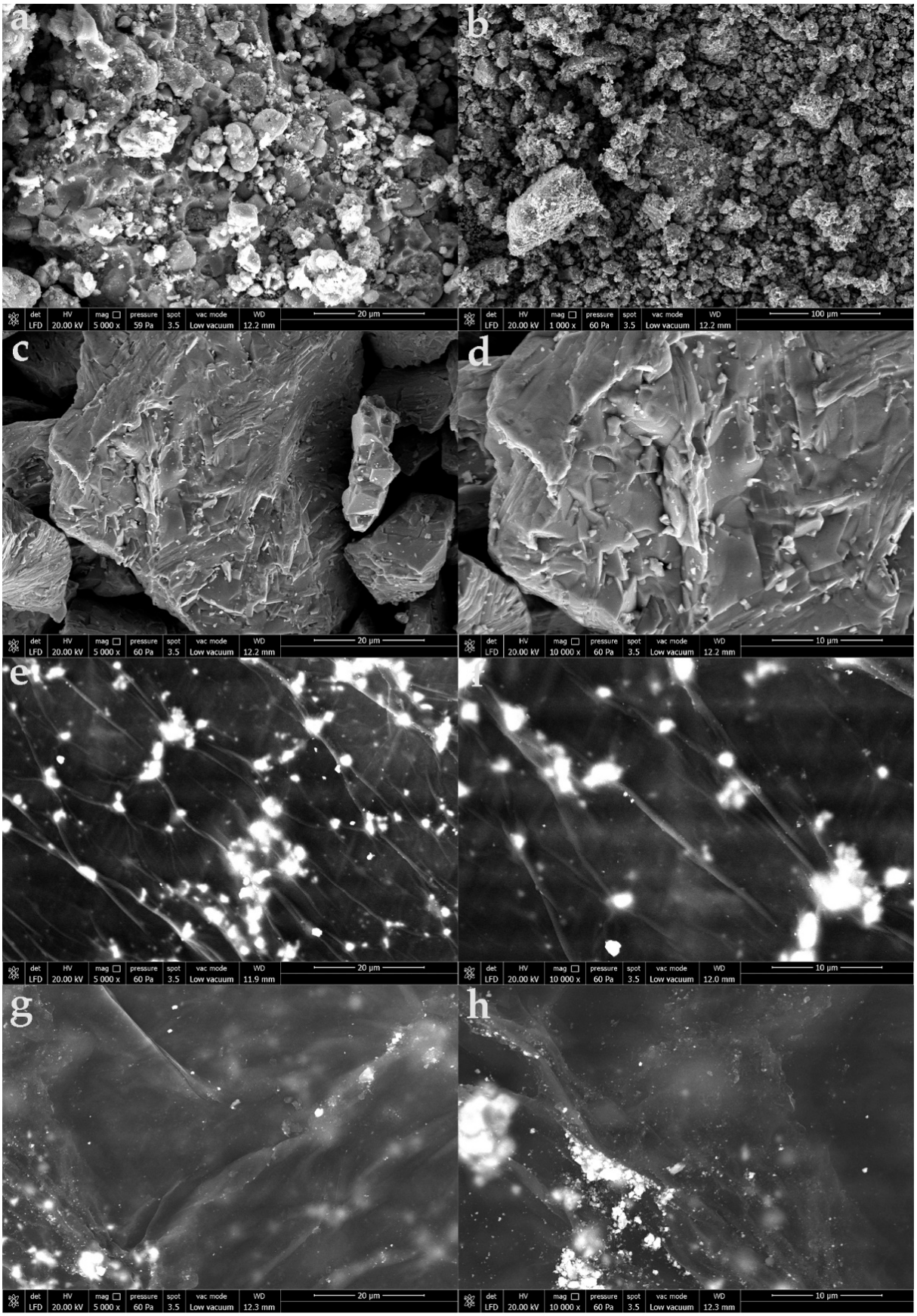

Figure 5. SEM images of WO_3 (**a**,**b**), WC (**c**,**d**), WO_3/GO ex situ synthesis (**e**,**f**), and WO_3/GO in situ synthesis (**g**,**h**).

The EDS analysis of WO_3 powders shows a tungsten atomic percentage of 79.35% and an oxygen atomic percentage of 20.65%. WC powders show tungsten at 90.34% and a carbon atomic percentage of 9.66%. After the synthesis of nanocomposites, a notable decrease in the atomic percentages of W elements was observed. Furthermore, the presence of GO was confirmed via EDS analyses, which showed additional carbon elements and oxygen elements in WO_3/GO ex situ and in situ, respectively (Table 1).

Table 1. Elemental composition of WO_3, WC and WO_3/GO in ex situ synthesis and in WO_3/GO in situ synthesis.

Samples	**% at.**		
	Oxygen	Tungsten	Carbon
WO_3	20.65	79.35	-
WC	-	90.34	9.66
WO_3/GO ex situ	41.10	8.62	50.28
WO_3/GO in situ	26.97	16.71	56.32

Figure 6 shows the XRD patterns of the ex situ and in situ WO_3/GO, WO_3/GO nanocomposites, which confirms the presence of both WO_3 and GO.

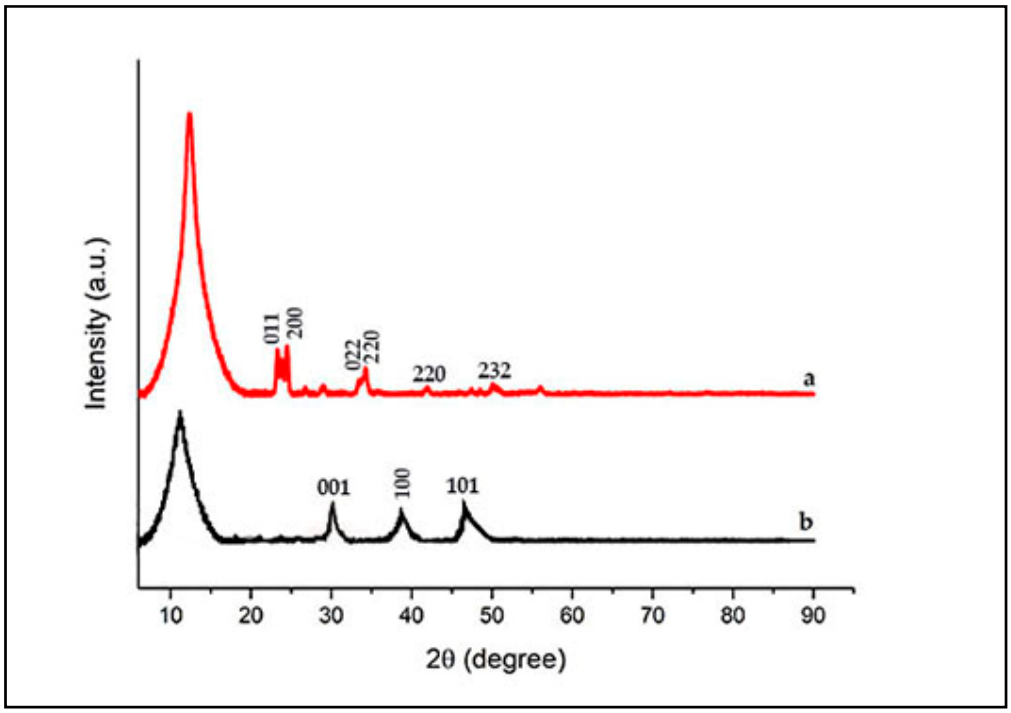

Figure 6. XRD patterns of WO_3/GO ex situ synthesis (a) and WO_3/GO in situ synthesis (b).

A low intensity peak at 10.8° indicates the formation of GO sheets in the in situ synthesis of WO_3/GO, which is due to the poor crystalline nature of carbon. The other peaks at 2θ values of 23.3, 24.5, 34.2, 42.1, 47.49, and 50.22 confirm the presence of WO_3 particles [39].

The WC diffraction spectrum shows three major intense peaks located at 2θ = 30.42°, 38.98°, and 47.03°, which correspond well to the crystallographic planes (001, 100, and 101) of WC, respectively [40].

3.3. Photocatalytic Degradation

Figure 7 shows the adsorption capacities (q_e) of WO_3 and WO_3/GO ex situ and WO_3/GO in situ nanocomposites, which were calculated using the following formula:

$$q_e = \frac{C_0 - C_e}{m} * V$$

where C_0 (mg/L) and C_e (mg/L) refer, respectively, to the initial concentration of the coloring agent and the concentration of the coloring agent remaining in the solution after adsorption, m (g) refers to the amount of adsorbents, and V (mL) represents the volume of the solution. Accordingly, WO_3 showed adsorption capacities in the range of 12.65–15.59, while WO_3/GO ex situ and WO_3/GO in situ nanocomposites showed adsorption capacities in the range of 15.18–19.84 and 19.46–23.91, respectively. During the experiment, the adsorption maximum capacity was determined with WO_3/GO in situ nanocomposites at t = 270, and the lowest was determined with WO_3 at t = 0. Within the increasing time intervals, the adsorption capacity of WO_3/GO in situ nanocomposites showed a significant increase after 3 h. This shows that this situation can be associated with the surface area of the nanocomposite, thus leading to the understanding that the photocatalytic effect increases with time.

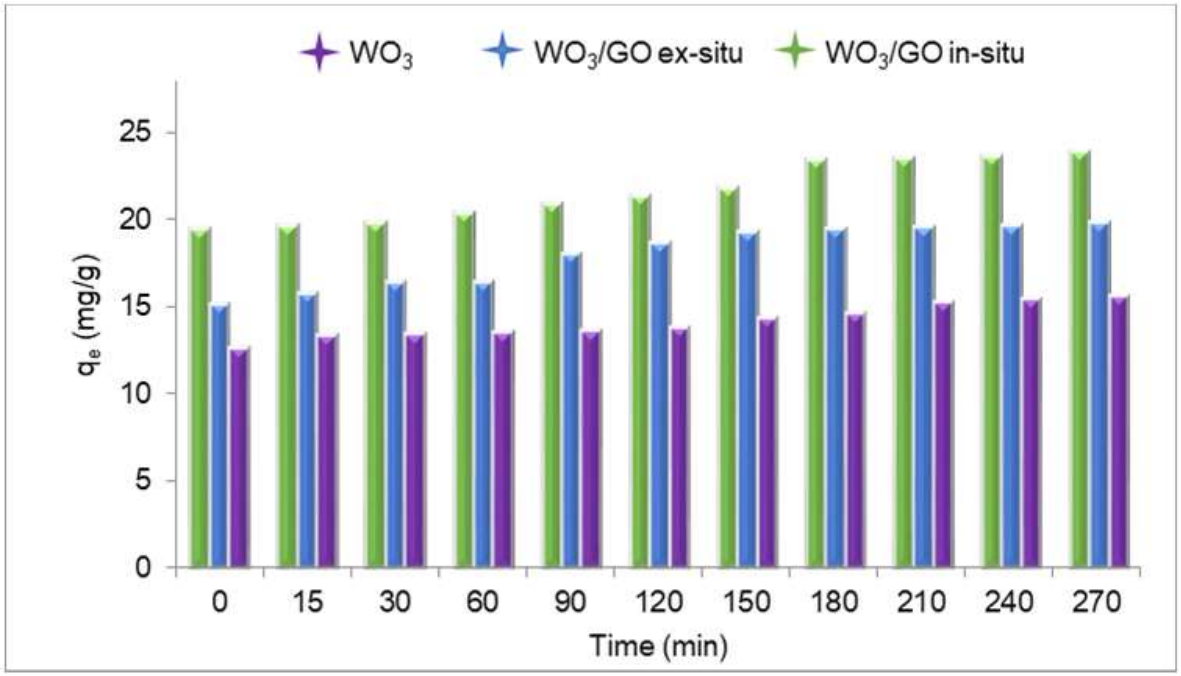

Figure 7. Relationship between adsorption capacity and time.

The degradation efficiency of was calculated using the following formula:

$$\eta\% = \left(1 - \frac{C}{C_0}\right) \times 100$$

where C_0 is the absorption maximum at t = 0, and C is the absorption maximum after complete degradation.

WO_3 and WO_3/GO nanocomposites synthesized ex situ/in situ showed the maximum degradation of 75.79%, 90.52%, and 96.30% respectively (Figure 8). It was observed that the degradation amount of the WO_3/GO in situ catalyst was higher than the one of ex situ synthesis, and it was concluded that this difference depends on the synthesis method. When GO is added to the matrix, it increased the photocatalytic effect, and in parallel

with this, the synthesized nanocomposite structures reach higher percentage degradation efficiency values in a shorter time compared to WO_3.

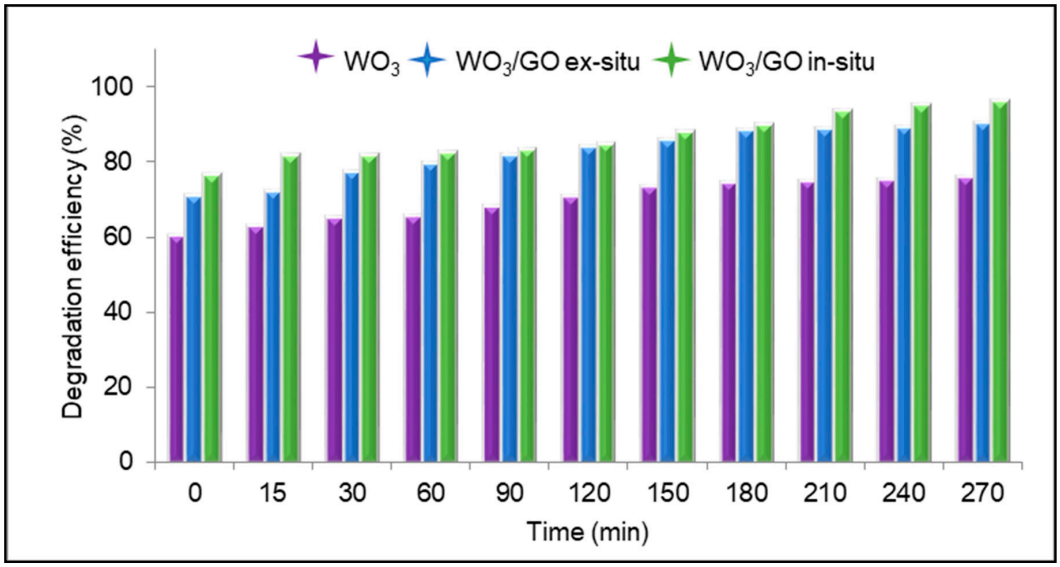

Figure 8. Degradation efficiency of MB.

The chemical structure of MB has cationic atoms and aromatic rings. The degradation mechanism starts with the MB dye adsorption on the nanocomposite's surface followed by its photodegradation, which can be summarized in the following steps. Figure 9 illustrates the mechanism of the photocatalytic degradation of MB via the WO_3/GO nanocomposite's UV irradiation. First, visible light radiation allows the transfer of electrons in in the valence band WO_3 to the conduction band of GO. Therefore, holes (h) and electrons (e-) are formed on the surface of the WO_3 photocatalyst. GO behaves as an electron acceptor via electrostatic and $\pi-\pi$ stacking interactions. Then, while the holes react with the hydroxide ion, the electrons react with dissolved oxygen to produce OH^-, which degrades MB dyes into non-toxic gases such as carbon dioxide and water. In addition, hydrogen peroxide reacts with electrons to produce more OH- to increase the degradation of the dye.

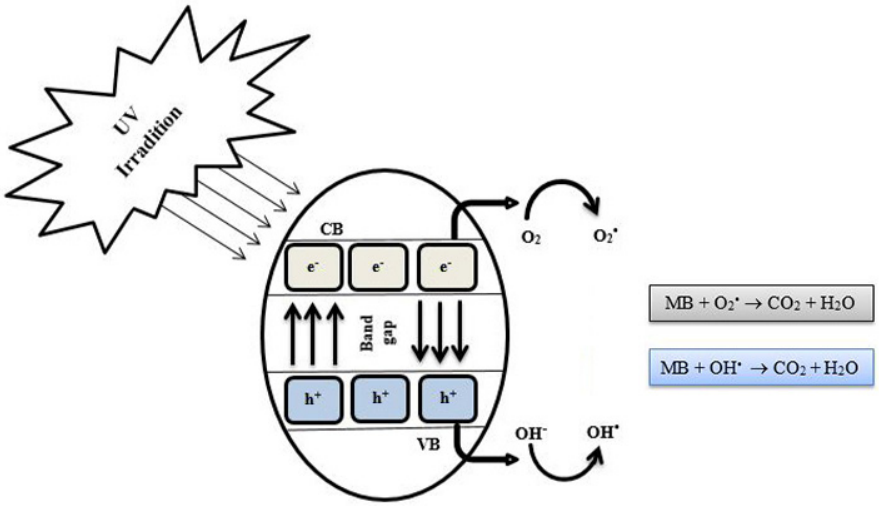

Figure 9. Schematic representation of photocatalytic degradation of methylene blue by WO_3/GO nanocomposites under UV irradiation illumination.

As shown in Table 2, prepared photocatalysts were compared with other WO_3-based nanocomposites. Their photocatalytic efficiency is usually at 80–97%. In this work,

WO_3/GO nanocomposites prepared by in situ synthesis were higher than that of the tungsten-oxide-based counterparts. In addition, the method is simple and does not require synthesizing GO separately; the in situ oxidation of graphite is provided while the nanocomposite is formed.

Table 2. Comparison of photocatalytic performance between this work and reported references.

Photocatalyst	Methods of Synthesis	Photodecomposition	Photocatalytic Effciency	References
WO_3/GO	In situ ex situ chemical oxidation	MB	96.30% 90.52%	Current work
WO_3/GO	Ultrasonication Method	MB	97.03%	[28]
WO_3/GO	Sol-gel method	MB	82%	[31]
WO_3/GO	Photo-reduction method	MO	92.7%	[32]
WO_3/GR	Hydrothermal method	MB	83%	[39]
WO_3/rGO	In situ slvothermal method	MB	94%	[41]

4. Discussion

The photocatalytic activities of the WO_3 and WO_3/GO nanocomposites were evaluated by the degradation of MB in aqueous solutions. Compared with WO_3, the photocatalytic activity of the WO_3/GO nanocomposites was enhanced, and the best degradation efficiencies for MB was 96.30% for the WO_3/GO in situ synthesis nanocomposite. It was attributed to the large surface area of GO, which served as an acceptor of the electrons generated in the WO_3 and effectively decreased the recombination. To overcome the rapid recombination and slow migration of charge carriers, different morphologies have been developed, such as nanoplates, nanotubes, and nano-sheets. The homogeneous nanoplate structure formed in in situ syntheses showed higher photocatalytic effects due to its large surface area than the nanorod-like structure formed as a result of ex situ syntheses.

Although there are various different pollutant sources in the environment [42], the application of composite-based photocatalysts is limited to water treatments. Expanding the application areas of GO-based photocatalysts with different studies is necessary. Laboratory equipment is mostly used for the degradation processes in the laboratory. To prepare photocatalysts on a commercial scale, cost studies should be carried out for the large-scale degradation of pollutants, and systems should be modified with appropriate strategies. It is seen that suitable morphologies can be obtained by adjusting different methods and reaction conditions, and morphology control is an important parameter for photocatalytic activities.

5. Conclusions

In summary, we reported a simple chemical in situ and ex situ synthesis process and the physical properties and photocatalytic activities of WO_3/GO composite structures. We observed that different synthesis methods affect WO_3/GO's morphology, while different WO_3/GO morphologies affect photocatalytic performances. The ex situ preparation of the composite leads to the formation of well-dispersed WO_3 with smoother surface in the WO_3/GO. However, the in situ-prepared WO_3 nanostructures have showed that single-phase homogeneous composite morphologies formed with good interfacial interactions between GO and WC. The prepared WO_3 and its nanocomposite with GO was evidenced for the dye degradation of MB. The best degradation efficiencies for MB were 96.30% for the WO_3/GO in situ synthesis nanocomposite, which are much better than that of WO_3. The results showed that WO_3/GO composites exhibited an enhanced WO_3 photocatalysis efficiency in visible light. This study gave a new perspective for applications of WO_3/GO nanocomposite photocatalysts for various areas.

Author Contributions: Conceptualization, B.E.T. and A.K.Ç.; methodology B.E.T., A.K.Ç. and N.F.; validation, B.E.T., A.D. and A.K.Ç.; formal analysis, N.F.; investigation, B.E.T. and A.D.; resources, B.E.T. and A.D.; data curation, B.E.T. and A.D.; writing—original draft preparation, B.E.T., A.D. and N.F.; writing—review and editing, B.E.T. and N.F.; visualization, B.E.T. and A.D.; supervision, B.E.T. and N.F.; project administration, B.E.T., A.K.Ç., A.D. and N.F. All authors have read and agreed to the published version of the manuscript.

Funding: This research was funded by grants from the Scientific and Technological Research Council of Turkey (TUBITAK, project code: 1919B012001762).

Institutional Review Board Statement: Not applicable.

Informed Consent Statement: Not applicable.

Data Availability Statement: Not applicable.

Conflicts of Interest: The authors declare no conflict of interest.

References

1. Alam, M.W.; Aamir, M.; Farhan, M.; Albuhulayqah, M.; Ahmad, M.M.; Ravikumar, C.; Dileep Kumar, V.; Ananda Murthy, H. Green Synthesis of Ni-Cu-Zn Based Nanosized Metal Oxides for Photocatalytic and Sensor Applications. *Crystals* **2021**, *11*, 1467. [CrossRef]
2. Hossain, S.; Chu, W.S.; Lee, C.S.; Ahn, S.H.; Chun, D.M. Photocatalytic performance of few-layer Graphene/WO_3 thin films prepared by a nano-particle deposition system. *Mater. Chem. Phys.* **2019**, *226*, 141–150. [CrossRef]
3. Alam, M.W.; Al Qahtani, H.S.; Souayeh, B.; Ahmed, W.; Albalawi, H.; Farhan, M.; Abuzir, A.; Naeem, S. Novel Copper-Zinc-Manganese Ternary Metal Oxide Nanocomposite as Heterogeneous Catalyst for Glucose Sensor and Antibacterial Activity. *Antioxidants* **2022**, *11*, 1064. [CrossRef] [PubMed]
4. Chatterjee, S.G.; Chatterjee, S.; Ray, A.K.; Chakraborty, A.K. Graphene–metal oxide nanohybrids for toxic gas sensor. *Sens. Actuators B Chem.* **2015**, *221*, 1170–1181. [CrossRef]
5. Chang, X.; Zhou, Q.; Sun, S.; Shao, C.; Lei, Y.; Liu, T.; Yin, Y. Graphene-tungsten oxide nanocomposites with highly enhanced gas-sensing performance. *J. Alloys Compd.* **2017**, *705*, 659–667. [CrossRef]
6. Tian, W.; Liu, X.; Yu, W. Research Progress of Gas Sensor Based on Graphene and Its Derivatives. *Appl. Sci.* **2018**, *8*, 1118. [CrossRef]
7. Zhang, J.; Liu, X.; Neri, G.; Pinna, N. Nanostructured materials for room-temperature gas sensors. *Adv. Mater.* **2016**, *28*, 795–831. [CrossRef]
8. Le, X.V.; Luu, T.L.A.; Nguyen, H.L.; Nguyen, C.T. Synergistic enhancement of ammonia gassensing properties at low temperature by compositing carbon nanotubes with tungsten oxide nanobricks. *Vacuum* **2019**, *168*, 108861. [CrossRef]
9. Korotcenkov, G.; Brinzari, V.; Ivanov, M.; Cerneavschi, A.; Rodríguez, J.R.; Cirera, A.; Cornet, A.; Morante, J.R. Structural stability of indium oxide films deposited by spray pyrolysis during thermal annealing. *Thin Solid Films* **2005**, *479*, 38–51. [CrossRef]
10. Righettoni, M.; Amann, A.; Pratsinis, S.E. Breath analysis by nanostructured metal oxides as chemoresistive gas sensors. *Mater. Today* **2015**, *18*, 163–171. [CrossRef]
11. Sayama, K.; Hayashi, H.; Arai, T.; Yanagida, M.; Gunji, T.; Sugihara, H. Highly active WO_3 semiconductor photocatalyst prepared from amorphous peroxo-tungstic acid for the degradation of various organic compounds. *Appl. Catal. B Environ.* **2010**, *94*, 150–157. [CrossRef]
12. Guo, Y.; Quan, X.; Lu, N.; Zhao, H.; Chen, S. High photocatalytic capability of self-assembled nanoporous WO_3 with preferential orientation of (002) planes. *Environ. Sci. Technol.* **2007**, *41*, 4422–4427. [CrossRef] [PubMed]
13. Sonia, S.; Kumar, P.S.; Mangalaraj, D.; Ponpandian, N.; Viswanathan, C. Influence of growth and photocatalytic properties of copper selenide (CuSe) nanoparticles using reflux condensation method. *Appl. Surf. Sci.* **2013**, *283*, 802–807. [CrossRef]
14. Deng, F.; Pei, X.; Luo, Y.; Luo, X.; Dionysiou, D.D.; Wu, S.; Luo, S. Fabrication of hierarchically porous reduced graphene oxide/SnIn4S8 composites by a low-temperature coprecipitation strategy and their excellent visible-light photocatalytic mineralization performance. *Catalysts* **2016**, *6*, 113. [CrossRef]
15. Sun, S.; Wang, W.; Zeng, S.; Shang, M.; Zhang, L. Preparation of ordered mesoporous Ag/WO_3 and its highly efficient degradation of acetaldehyde under visible-light irradiation. *J. Hazard. Mater.* **2010**, *178*, 427–433. [CrossRef]
16. Zheng, H.; Mathe, M. Hydrogen evolution reaction on single crystal WO_3/C nanoparticles supported on carbon in acid and alkaline solution. *Int. J. Hydrogen Energy* **2011**, *36*, 1960–1964. [CrossRef]
17. Cao, L.; Yuan, J.; Chen, M.; Shangguan, W. Photocatalytic energy storage ability of TiO2-WO_3 composite prepared by wet-chemical technique. *Res. J. Environ. Sci.* **2010**, *22*, 454–459. [CrossRef]
18. Kalanur, S.S.; Seo, H. Aligned nanotriangles of tantalum doped tungsten oxide for improved photoelectrochemical water splitting. *J. Alloys Compd.* **2019**, *785*, 1097–1105. [CrossRef]
19. Chen, H.; Chen, Z.; Yang, H.; Wen, L.; Yi, Z.; Zhou, Z.; Dai, B.; Zhang, J.; Wu, X.; Wu, P. Multi-mode surface plasmon resonance absorber based on dart-type single-layer graphene. *RSC Adv.* **2022**, *12*, 7821–7829. [CrossRef]

20. Zhang, Z.; Cai, R.; Long, F.; Wang, J. Development and application of tetrabromobisphenol A imprinted electrochemical sensor based on graphene/carbon nanotubes three-dimensional nanocomposites modified carbon electrode. *Talanta* **2015**, *134*, 435–442. [CrossRef]
21. Shangguan, Q.; Chen, Z.; Yang, H.; Cheng, S.; Yang, W.; Yi, Z.; Wu, X.; Wang, S.; Yi, Y.; Wu, P. Design of Ultra-Narrow Band Graphene Refractive Index Sensor. *Sensors* **2022**, *22*, 6483. [CrossRef] [PubMed]
22. Alam, S.N.; Sharma, N.; Kumar, L. Synthesis of graphene oxide (GO) by modified hummers method and its thermal reduction to obtain reduced graphene oxide (rGO). *Graphene* **2017**, *6*, 1–18. [CrossRef]
23. Khan, Z.U.; Kausar, A.; Ullah, H.; Badshah, A.; Khan, W.U. A review of graphene oxide, graphene buckypaper, and polymer/graphene composites: Properties and fabrication techniques. *J. Plast. Film Sheeting* **2016**, *32*, 336–379. [CrossRef]
24. Cheng, Z.; Liao, J.; He, B.; Zhang, F.; Zhang, F.; Huang, X.; Zhou, L. One-Step Fabrication of Graphene Oxide Enhanced Magnetic Composite Gel for Highly Efficient Dye Adsorption and Catalysis. *ACS Sustain. Chem. Eng.* **2015**, *3*, 1677–1685. [CrossRef]
25. Hummers, W.S., Jr.; Offeman, R.E. Preparation of graphitic oxide. *J. Am. Chem. Soc.* **1958**, *80*, 1339. [CrossRef]
26. Yu, H.; Zhang, B.; Bulin, C.; Li, R.; Xing, R. High-efficient synthesis of graphene oxide based on improved hummers method. *Sci. Rep.* **2016**, *6*, 36143. [CrossRef] [PubMed]
27. Yazıcı, M.; Tiyek, İ.; Ersoy, M.S.; Alma, M.H.; Dönmez, U.; Yıldırım, B.; Salan, T.; Karataş, Ş.; Uruş, S.; Karteri, İ.; et al. Modifiye Hummers Yöntemiyle Grafen Oksit (GO) Sentezi ve Karakterizasyonu. *GU J. Sci. Part C* **2016**, *4*, 43–50.
28. Jeevitha, G.; Abhinayaa, R.; Mangalaraj, D.; Ponpandian, N. Tungsten oxide-graphene oxide (WO_3-GO) nanocomposite as an efficient photocatalyst, antibacterial and anticancer agent. *J. Phys. Chem. Solids* **2018**, *116*, 137–147. [CrossRef]
29. Fu, L.; Xia, T.; Zheng, Y.; Yang, J.; Wang, A.; Wang, Z. Preparation of WO_3-reduced graphene oxide nanocomposites with enhanced photocatalytic property. *Ceram. Int.* **2015**, *41*, 5903–5908. [CrossRef]
30. Kofuji, Y.; Isobe, Y.; Shiraishi, Y.; Sakamoto, H.; Ichikawa, S.; Tanaka, S.; Hirai, T. Hydrogen peroxide production on a carbon nitride–boron nitride-reduced graphene oxide hybrid photocatalyst under visible light. *ChemCatChem* **2018**, *10*, 2070–2077. [CrossRef]
31. Ismail, A.A.; Faisal, M.; Al-Haddad, A. Mesoporous WO_3-graphene photocatalyst for photocatalytic degradation of Methylene Blue dye under visible light illumination. *Res. J. Environ. Sci.* **2018**, *66*, 328–337. [CrossRef]
32. Zhou, M.; Yan, J.; Cui, P. Synthesis and enhanced photocatalytic performance of WO_3 nanorods@ graphene nanocomposites. *Mater. Lett.* **2012**, *89*, 258–261. [CrossRef]
33. Bragaglia, M.; Paleari, L.; Lamastra, F.R.; Puglia, D.; Fabbrocino, F.; Nanni, F. Graphene nanoplatelet, multiwall carbon nanotube, and hybrid multiwall carbon nanotube–graphene nanoplatelet epoxy nanocomposites as strain sensing coatings. *J. Reinf. Plast. Compos.* **2021**, *40*, 632–643. [CrossRef]
34. Pittella, E.; D'Alvia, L.; Palermo, E.; Piuzzi, E. Microwave Characterization of 3D Printed PLA and PLA/CNT Composites. In Proceedings of the 2021 IEEE 6th International Forum on Research and Technology for Society and Industry (RTSI), Rome, Italy, 7–9 June 2021. [CrossRef]
35. Paleari, L.; Bragaglia, M.; Fabbrocino, F.; Nanni, F. Structural Monitoring of Glass Fiber/Epoxy Laminates by Means of Carbon Nanotubes and Carbon Black Self-Monitoring Plies. *Nanomaterials* **2021**, *11*, 1543. [CrossRef]
36. Izadi, R.; Tuna, M.; Trovalusci, P.; Ghavanloo, E. Torsional Characteristics of Carbon Nanotubes: Micropolar Elasticity Models and Molecular Dynamics Simulation. *Nanomaterials* **2021**, *11*, 453. [CrossRef] [PubMed]
37. Hanifah, M.F.R.; Jaafar, J.; Aziz, M.; Ismail, A.F.; Rahman, M.A.; Othman, M.H.D. Synthesis of kaphene oxide nanosheets via modified hummers method and ıts physicochemical properties. *J. Technol.* **2015**, *74*, 189–192. [CrossRef]
38. Murugan Vadivel, A.; Muraliganth, T.; Manthiram, A. Rapid, Facile Microwave-Solvothermal Synthesis of Graphene Nanosheets and Their Polyaniline Nanocomposites for Energy Strorage. *Chem. Mater.* **2009**, *21*, 5004–5006. [CrossRef]
39. Hu, X.; Xu, P.; Gong, H.; Yin, G. Synthesis and Characterization of WO_3/Graphene Nanocomposites for Enhanced Photo-catalytic Activities by One-Step In-Situ Hydrothermal Reaction. *Materials* **2018**, *11*, 147. [CrossRef]
40. Vakhrushev, A.V. Synthesis of WO_3 Nanostructures and Their Nanocomposites with Graphene Derivatives via Novel Chemical Approach. In *Nanomechanics—Theory and Application*; IntechOpen: London, UK, 2021; 146p. [CrossRef]
41. Tie, L.; Yu, C.; Zhao, Y.; Chen, H.; Yang, S.; Sun, J.; Dong, S.; Sun, J. Fabrication of WO_3 na-norods on reduced graphene oxide sheets with augmented visible light photocatalytic ac-tivity for efficient mineralization of dye. *J. Alloys Compd.* **2018**, *769*, 83–91. [CrossRef]
42. Derradji, M.; Mehelli, O.; Liu, W.; Fantuzzi, N. Sustainable and Ecofriendly Chemical Design of High Performance Bio-Based Thermosets for Advanced Applications. *Front. Chem.* **2021**, *9*, 691117. [CrossRef]